A Moderate Online Servo Controller Parameter Self-Tuning Method via Variable-Period Inertia Identification

Yangyang Chen, Ming Yang, *Senior Member, IEEE*, Jiang Long, Wanying Qu, Dianguo Xu, *Fellow, IEEE*, and Frede Blaabjerg, *Fellow, IEEE*

***Abstract*—As universal servos are economical, they are chosen for most of the industrial applications. However, tuning them accurately poses some challenges. Accurate electrical and mechanical parameters are essential for a model-based high-performance servo controller design. In motion control, the variation of inertia is much more significant than that of other parameters. Thus, inertia identification is a key to effective online controller parameter self-tuning, but most conventional inertia-identification methods cannot be well applied in some complicated situations, such as those caused by irregularly and slowly varying speed. Additionally, the traditional control parameter tuning theory displays a deep understanding of the relationship between controller gain and inertia, but lacks an analysis of the maximum bandwidth of the system. In this paper, based on a widely accepted structure that is composed of inertia identification and online controller self-tuning, several simple but useful modifications are proposed. First, to reduce the noise from an encoder quantization error and thus to improve the accuracy of inertia identification, a motor acceleration calculation method featuring an inconstant period is proposed. Then, the scope of the application is extended to make it suitable for position control by redesigning the inertia updating time of the conventional method. In addition, to guarantee the stability of servo systems, the upper constraint of the expected maximum system bandwidth is derived by taking the controller saturation nonlinearity and hardware capacity into consideration. Finally, a modified moderate systematic online servo controller parameter self-tuning method via variable-period inertia identification is presented. The validity, effectiveness, and advantages of proposed strategies are verified by several experimental results.**

***Index Terms*—Inertia identification, self-tuning, servo drive.**

Manuscript received September 25, 2018; revised December 8, 2018 and February 18, 2019; accepted March 24, 2019. Date of publication April 3, 2019; date of current version September 6, 2019. This work was supported in part by the National Key R&D Program of China under Grant 2017YFB1300801 and the Power Electronics Science and Education Development Program of Delta Environmental and Educational Foundation under Grant DREK2017004. Recommended for publication by Associate Editor S. K. Panda. *(Corresponding author: Ming Yang.)*

Y. Chen, M. Yang, J. Long, W. Qu, and D. Xu are with the School of Electrical Engineering and Automation, Harbin Institute of Technology, Harbin 150001, China (e-mail:

servos, the combination of simple but robust PID controllers and low-cost microchips is more suitable. In this paper, the universal servo, which has a larger market share, is the research focus.

There are two methods for universal servo PID controller self-tuning—rule-based and model-based. In general, for the rule-based methods, several indices such as the integral of squared error, the integral of weighted time absolute error, the overshoot cost function, and others are predetermined for performance evaluation [18], [21], [22]. However, this method poses challenges in terms of setting parameters. Although after training and learning this method can result in optimal parameters, the assignment of the indices' weight, the design of the searching process, and the setting of controllers' initial values are additional factors that must be undertaken with care. The time-domain response-based Ziegler–Nichols parameter-tuning rule is simple, but its performance is relatively fixed and it cannot cope with systems having time-varying model parameters. The second type of servo controller self-tuning is the model-based method [4], [23]–[27]. In this method, because of the uncertainty and time-varying problems of the model parameters [28]–[31], a relatively simplified motor drive model is built and the controller can calculate the control parameters by itself based on the predetermined or observed model state variables. Since, for universal servos, the electrical parameters of the motor are fixed in most situations, the current controller can be predetermined. In addition, inertia is the decisive factor for the design of the outer loop controllers (the speed controller and the position controller). Hence, the simpler and more straightforward inertia observer-based self-tuning controller is preferable in commercial servo drives, and the accuracy of observed inertia will directly affect the control performance.

The conventional inertia observation can also be classified into two groups—offline identification and online identification. Offline identification is used only in limited circumstances. Because offline inertia identification is needed to operate the system under certain references, this method only can be applied in the commissioning process and is only suitable for systems with fixed inertia [4], [23], [24], [32]–[38]. As opposed to the offline strategy, the online inertia identification can cover more complicated situations, but these complicated situations bring their own set of complications. During the operation of servo systems in real applications, both the moment of inertia and the load torque are uncertain without preestimation or modeling. Thus, online inertia observation needs to deal with simultaneous changes in torque and inertia. To solve this problem, the online identification of inertia can be divided into two categories. The first type is to build up a high-order observer or a multialgorithm composite structure to achieve real-time inertia and torque identifications [7], [25], [31], [39]–[41], but the fluctuation of transient-state observation results and the verification of the asymptotic convergence are still problems that need to be solved. In response, the second type of algorithm was proposed by Awaya *et al*. (Mitsubishi Heavy Industries Ltd.) in 1992 [42]. Their main idea is to use the integration method to counteract the influence that comes from uncertain load torque, and to periodically update the observed inertia. This method can identify inertia smoothly and has a stronger antinoise ability [21], [27], [42]. However, this method is limited because periodic motor speed and constant or slow-varying load torque are preconditions for using this method. Based on this classic method, Kwon *et al*. [43] deduced a set of derivational formulas to simultaneously identify the viscous friction coefficient and inertia. In addition, Li and Liu [14], and Kim *et al*. [44] added different controllers or disturbance observers into the conventional structure to achieve better disturbance compensation and instantaneous speed observations, but the algorithm complexity was increased as a tradeoff. In this paper, the second type of integration form of online inertia-identification method is adopted, because it is simpler and more mature.

Overall, the model-based parameter self-tuning method, discussed in this paper, comprises two main steps—online inertia identification and parameter calculation. In general, this structure still has some shortcomings.

1) The motor speed variation is necessary for inertia identification, but a rapid change in motor speed is unacceptable in systems with high-precision optical measuring equipment and elastic terminal tools (for example, inspection flow-line for cell phone and lens), or fragile manufacture objects (wire-drawing machine). In the medium- to low-end universal servos equipped with the cost-effective encoders, the quantization error from the encoder can drown out the real speed differential information when speed changes slowly, despite the noise-reduction ability of the integration method.
2) The periodic speed precondition of the integration inertia identification is still too strict for normal industrial manufacturing. Most of the times, users' commands of the motor angle position and speed are irregular.
3) After inertia identification is finished, according to the classic linear control theory, the proportional gain of the position controller is independent of inertia. Meanwhile, the proportional gain of the speed controller is in a positive proportion to inertia when the expectation of the controller bandwidth is fixed. In the condition where load inertia is large, unboundedly increasing control gain is inadvisable, but few sources give bandwidth-tuning guidance or discuss the relationship between a system's inertia and the maximum bandwidth.

Thus, a further extension of this method is needed. In this paper, a brief introduction of the classic inertia-identification theory and conventional model–based parameter-tuning method is given at first. Next, considering that any innovation can be a threat for the stability of commercial servo products, rather than overthrowing the entire classic algorithmic architecture, three simple but useful targeted improvement strategies are proposed. It is worth mentioning that, these three modification methods can be used independently. Moreover, the first and the third one can also be applied to other types of inertia-identification strategies and model-based parameter self-tuning methods.

1) An easily implemented variable-period inertia-identifi cation strategy is proposed to weaken the quantization error from speed measurement.

2) Through a combination of the speed zero-cross characteristics in a position mode, the periodic inertia update condition is redefined to enlarge the application field of this method.
3) A comprehensive modeling of the relationship between inertia, control gain, and the maximum bandwidth is finished. The physical limit constraint, linear control constraint, and hardware maximum bandwidth constraint are derived. Analysis verifies that the maximum bandwidth is limited by the controller saturation nonlinearity and hardware capability, and these maximum bandwidth constraints are used to fix the expected bandwidth from users to achieve a moderate control performance.

Experimental results demonstrate that the improved parameters self-tuning and inertia-identification strategies are more widely applicable, more stable, and with stronger antinoise ability.

II. Traditional Inertia-Identification and Controller Parameters Self-Tuning Method

In order to provide a context for analyzing in-depth the residue problems posed by the conventional model-based controller self-tuning algorithm, the classic theory of inertia identification and a typical parameter calculation method (including the speed controller and the position controller) are introduced in this part.

A. Inertia Identification

Inertia identification is the first step in controller parameter tuning. Its accuracy is directly related to the performance of the motor drive. Hence, the integration inertia identification is adopted to get a smooth and highly accurate inertia observation result. The kinematics equation for the traditional inertia identification can be given as

$$T_e(t) = \hat{J}\frac{d\omega_m(t)}{dt} + \Delta J\frac{d\omega_m(t)}{dt} + B\omega_m(t) + T_L = \hat{J}\frac{d\omega_m(t)}{dt} + \hat{T}_r(t) \tag{1}$$

in which T_e is electrical torque, $\hat{J}$ is observed inertia, ΔJ is the observation error of inertia, B is the damping coefficient, and ω_m is the motor speed. T_L is the disturbance torque and it is assumed that it varies slowly. This formula regards those items related to ΔJ, B, and T_L as an equivalent disturbance torque $\hat{T}_r(t)$ [27], [42]–[44].

By multiplying by angular acceleration, $d\omega_m/dt$, on both sides of the expression of $\hat{T}_r(t)$, (1) can be rewritten as

$$\hat{T}_r(t)\frac{d\omega_m(t)}{dt} = \Delta J\left(\frac{d\omega_m(t)}{dt}\right)^2 + B\omega_m(t)\frac{d\omega_m(t)}{dt} + T_L\frac{d\omega_m(t)}{dt}. \tag{2}$$

Then by integrating both sides of (2), the integration form of the torque equation can be given as

$$\int_{t_1}^{t_2}\hat{T}_r(t)\frac{d\omega_m(t)}{dt}dt = \Delta J\int_{t_1}^{t_2}\left(\frac{d\omega_m(t)}{dt}\right)^2 dt + B\int_{t_1}^{t_2}\omega_m(t)\frac{d\omega_m(t)}{dt}dt + T_L\int_{t_1}^{t_2}\frac{d\omega_m(t)}{dt}dt \tag{3}$$

where t_1 and t_2 are the initial time point and the ending time point of the estimation process, respectively. The second term and the third term on the right-hand side of (3) can be expressed as

$$\begin{cases} B\displaystyle\int_{t_1}^{t_2}\omega_m(t)\frac{d\omega_m(t)}{dt}dt = \frac{B}{2}\left(\omega_m(t_2)^2 - \omega_m(t_1)^2\right) \\ T_L\displaystyle\int_{t_1}^{t_2}\frac{d\omega_m(t)}{dt}dt = T_L\left(\omega_m(t_2) - \omega_m(t_1)\right). \end{cases} \tag{4}$$

By substituting (4) into (3), the inertia estimation error ΔJ can be identified by

$$\Delta J = \frac{\int_{t_1}^{t_2}\hat{T}_r(t)\frac{d\omega_m(t)}{dt}dt}{\int_{t_1}^{t_2}\left(\frac{d\omega_m(t)}{dt}\right)^2 dt} - \frac{B}{2}\frac{\left(\omega_m(t_2)^2 - \omega_m(t_1)^2\right)}{\int_{t_1}^{t_2}\left(\frac{d\omega_m(t)}{dt}\right)^2 dt} - T_L\frac{\left(\omega_m(t_2) - \omega_m(t_1)\right)}{\int_{t_1}^{t_2}\left(\frac{d\omega_m(t)}{dt}\right)^2 dt}. \tag{5}$$

As seen from (5), if the estimation time defined as $t_2 - t_1$ is long enough, the denominators on the right-hand side of (5) are large enough to neglect the second and third terms on the right-hand side of (5). Thus, the first term by itself is enough to estimate the inertia error or variation ΔJ. In particular, if the speeds at t_1 and at t_2 are the same, the second and the third terms should be zero. Then the inertia can be estimated only by the first term without the approximation error. Hence, assuming the motor speed is periodic and its period is T_p

$$\omega_m(t) = \omega_m(t + T_p), \quad \frac{d\omega_m(t)}{dt} \not\equiv 0. \tag{6}$$

Because (6) exists, the last two items on the right of (5) can be calculated as $(k \in N^+)$

$$\begin{cases} \dfrac{B}{2}\dfrac{\left(\omega_m(kT_p)^2 - \omega_m((k-1)T_p)^2\right)}{\int_{(k-1)T_p}^{kT_p}\left(\frac{d\omega_m(t)}{dt}\right)^2 dt} = 0 \\ T_L\dfrac{\left(\omega_m(kT_p) - \omega_m((k-1)T_p)\right)}{\int_{(k-1)T_p}^{kT_p}\left(\frac{d\omega_m(t)}{dt}\right)^2 dt} = 0. \end{cases} \tag{7}$$

Finally, by substituting (7) into (5), the classic inertia-identification recursion formula can be given as

$$\hat{J}(k) = \hat{J}(k-1) + \Delta J = \hat{J}(k-1) + \frac{\int_{(k-1)T_p}^{kT_p}\hat{T}_r(t)\frac{d\omega_m(t)}{dt}dt}{\int_{(k-1)T_p}^{kT_p}\left(\frac{d\omega_m(t)}{dt}\right)^2 dt}. \tag{8}$$

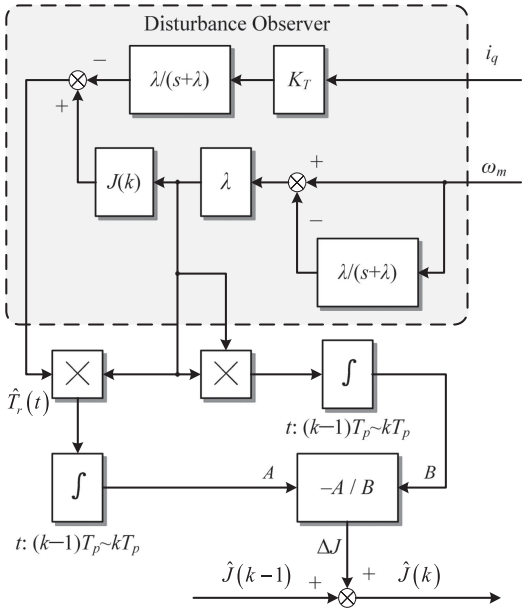

Fig. 1. Block diagram of inertia identification.

The block diagram showing inertia identification is given in Fig. 1. Besides inertia estimation, the entire structure also includes a simple disturbance observer [14], [42]. The filter factor is represented by λ.

The convergence proof of this type of inertia identification is given in references [27], [42], and [44]. Overall, this method has following four prerequisites:

1) The motor torque constant K_t needs to be accurate.
2) The disturbance torque T_L and the inertia *J* can be uncertain, but should be constant or vary slowly in each period.
3) In order to achieve highly accurate inertia estimation, the motor angular acceleration $d\omega_m/dt$ should be large enough to reduce the influence of the measurement error from the encoder.
4) The velocity command of the servo system needs to be periodic and the entire system needs to reach a steady state to guarantee the validity of (6).

To expand the application range of this classic method, we propose a differential calculation method and a redesigned inertia update condition, which can eliminate or weaken the restrictions from the third and fourth prerequisites mentioned above. A full discussion is given in Section III of this paper.

B. Speed Loop Controller Parameter Self-Tuning

After inertia identification, controller parameter self-tuning begins with the calculation of the speed-regulator parameters. Considering that the speed differential noise, which is caused by cost-effective encoders and communication delays, will affect the stability of the system, a proportion-integration (PI) controller is used for speed control in this part [4], [26], [27]. Fig. 2 is the block diagram of the speed loop, in which the current loop is equaled to a torque constant K_T. $G_{\mathrm{ASR}}(s)$ is the transfer function of the speed controller. $\omega_{m\mathrm{ref}}$ and ω_m represent the speed reference and the motor speed, respectively. Electrical torque T_e

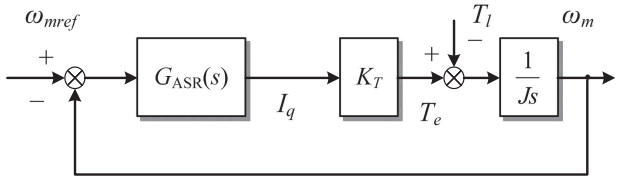

Fig. 2. Block diagram of speed loop system.

is proportional to the current in the direction of the quadrature direction i_q. T_e and load torque T_l both impose on the motor inertia *J*, thus making speed variation.

The transfer function of the speed controller $G_{\mathrm{ASR}}(s)$ can be expressed as

$$G_{\mathrm{ASR}}(s) = K_{\mathrm{sp}}\left(1 + \frac{K_{\mathrm{si}}}{s}\right) \tag{9}$$

in which K_{sp} and K_{si} represent proportional and integral gain, respectively.

According to Fig. 2, the open-loop transfer function of the speed loop $G_{\mathrm{so}}(s)$ can be given as

$$G_{\mathrm{so}}(s) = \frac{K_T K_{\mathrm{sp}} K_{\mathrm{si}}}{Js^2} \cdot \left(\frac{s}{K_{\mathrm{si}}} + 1\right). \tag{10}$$

Setting ω_{sc}^* as the open-loop cutoff frequency of the speed loop, φ_{sm} as the phase margin, and *u* as the phase margin coefficient of the speed loop, the phase margin equations of the speed loop can be given as

$$\begin{cases} |G_{\mathrm{so}}(j\omega_{\mathrm{sc}}^*)| = \dfrac{K_T K_{\mathrm{sp}} K_{\mathrm{si}} \sqrt{\left(\omega_{\mathrm{sc}}^*/K_{\mathrm{si}}\right)^2 + 1}}{J\omega_{\mathrm{sc}}^{*2}} = 1 \\ \angle G_{\mathrm{so}}(j\omega_{sc}^*) = \mathrm{atg}\left(\dfrac{\omega_{\mathrm{sc}}^*}{K_{\mathrm{si}}}\right) - \pi = \mathrm{atg}(u) - \pi = \varphi_{\mathrm{sm}} - \pi. \end{cases} \tag{11}$$

Considering that *u* is much larger than 1 to make the system stable and reduce overshoot, the item within the square root in (11) can be regarded as *u* to simplify the formula. Then, K_{sp} and K_{si} can be calculated as

$$\begin{cases} K_{\mathrm{si}} = \omega_{\mathrm{sc}}^*/u \\ K_{\mathrm{sp}} = \mathrm{J}\omega_{\mathrm{sc}}^*/\mathrm{K_T}. \end{cases} \tag{12}$$

In order to directly reflect the relationship between the closed-loop bandwidth and the controller parameters, a further derivation is needed. The closed-loop transfer function $G_{\mathrm{sc}}(s)$ and closed-loop cutoff frequency of the speed loop ω_{sc} can be given as

$$\begin{cases} G_{\mathrm{sc}}(s) = \dfrac{K_T K_{\mathrm{sp}} s + K_T K_{\mathrm{sp}} K_{\mathrm{si}}}{Js^2 + K_T K_{\mathrm{sp}} s + K_T K_{\mathrm{sp}} K_{\mathrm{si}}} \\ |G_{\mathrm{sc}}(j\omega_{\mathrm{sc}})| = 1/\sqrt{2}. \end{cases} \tag{13}$$

Substituting (12) into (13) yields

$$\omega_{\mathrm{sc}} = \omega_{\mathrm{sc}}^* \sqrt{\frac{(1+2/u) + \sqrt{8/u^2 + 4/u + 1}}{2}} = \omega_{\mathrm{sc}}^* u_{\mathrm{fix}} \tag{14}$$

in which u_{fix} is the proportional coefficient between ω_{sc} and ω_{sc}^*.

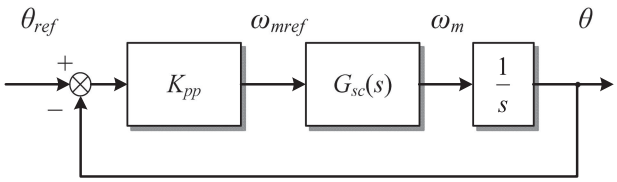

Fig. 3. Block diagram of position loop system.

By substituting (14) into (12), the equations of the speed controller parameters self-tuning can be given as

$$\begin{cases} K_{\mathrm{si}} = \omega_{\mathrm{sc}}/(uu_{\mathrm{fix}}) \\ K_{\mathrm{sp}} = J\omega_{\mathrm{sc}}/(K_T u_{\mathrm{fix}}) . \end{cases} \tag{15}$$

Setting T_{ASR} as the sampling period of the speed loop, K_{sidis} and K_{spdis} are the integral and proportional gain of the speed controller in the z-domain. Applying the Tustin transformation to discretize (15) and make the formula form to match with (9), the equations of speed controller parameters self-tuning can be rewritten as

$$\begin{cases} K_{\mathrm{sidis}} = \dfrac{2K_{\mathrm{si}}T_{\mathrm{ASR}}}{2 - K_{\mathrm{si}}T_{\mathrm{ASR}}} = \dfrac{2\omega_{\mathrm{sc}}T_{\mathrm{ASR}}}{2uu_{\mathrm{fix}} - \omega_{\mathrm{sc}}T_{\mathrm{ASR}}} \\ K_{\mathrm{spdis}} = K_{\mathrm{sp}} - \dfrac{K_{\mathrm{sp}}K_{\mathrm{si}}T_{\mathrm{ASR}}}{2} = \dfrac{J\omega_{\mathrm{sc}}}{K_T u_{\mathrm{fix}}} - \dfrac{J\omega_{\mathrm{sc}}^2 T_{\mathrm{ASR}}}{2K_T uu_{\mathrm{fix}}^2}. \end{cases} \tag{16}$$

C. Position Loop Controller Parameter Self-Tuning

Based on a speed regulator with good performance, position loop parameter tuning can be calculated. Fig. 3 is the block diagram of the position loop system. In order to simplify the operation, the inner loop $G_{\mathrm{sc}}(s)$ with higher bandwidth is represented by 1. K_{pp} represents the proportional gain of the position controller. θ_{ref} is the position reference and θ is the motor position. It should be noted that because a rational trajectory plan is a precondition for the performance of feedforward control, a discontinuous and mutated feedforward signal may lead to system vibration. However, because trajectory planning is not the focus of this paper, feedforward control is not used to simplify the algorithm.

The open-loop transfer function of system $G_{\mathrm{po}}(s)$ in Fig. 3 can be given as

$$G_{\mathrm{po}}(s) = K_{\mathrm{pp}}/s. \tag{17}$$

Similar to the derivation of the speed loop, setting ω_{pc}^* as the open-loop cutoff frequency of the position loop, the phase margin equations of the position loop can be given as

$$\begin{cases} \left|G_{\mathrm{po}}(j\omega_{\mathrm{pc}}^*)\right| = \dfrac{K_{\mathrm{pp}}}{\omega_{\mathrm{pc}}^*} = 1 \\ \angle G_{\mathrm{po}}(j\omega_{\mathrm{pc}}^*) = -\dfrac{\pi}{2}. \end{cases} \tag{18}$$

Because the closed-loop cutoff frequency ω_{pc} is equal to ω_{pc}^* for the integration function (17), K_{pp} can be calculated as

$$K_{\mathrm{pp}} = \omega_{\mathrm{pc}}. \tag{19}$$

Setting T_{APR} as the sampling period of the position loop, K_{ppdis} is the proportional gain of the position controller in the z-domain. Because no s exists in (19), the equation of the position controller parameter self-tuning in discrete domain can be expressed as

$$K_{\mathrm{ppdis}} = \omega_{\mathrm{pc}}. \tag{20}$$

III. Proposed Variable-Period Inertia-Identification Strategy

According to the analyses in Section II, a filter and the integration process are used in the conventional inertia-identification algorithm to get rid of the noise in the feedback signal, but it is still not enough. When the motor speed changes slowly, especially in those systems equipped with cost-effective encoders or which have relatively high sampling frequency, actual acceleration information will be submerged by quantization errors from the encoder. In addition, prerequisite (6) of the integration inertia identification method that "the command of the system needs to be periodic" is too strict for real industrial applications. In this part, a variable-period speed difference strategy and a redefinition mode of inertia update (in other words, variable-period inertia update) are proposed to cope with these two residual problems mentioned above.

A. Speed Differential Noise Analysis and Variable-Period Strategy

Rather than using a filter to deal with the existing noise, avoiding the generation of noise can be more effective. Hence, the analysis in this part is focused on finding a new acceleration calculation method to provide a cleaner input for inertia identification. Most conventional speed differential-based state value observers have fixed operation intervals (sampling periods). However, when the calculation period is fixed, the acceleration measurement error caused by the encoder is inversely related to the magnitude of the absolute value of the acceleration. Thus, it is difficult to estimate acceleration when speed changes slowly. In this section, a model for calculating speed differential noise is introduced, and then an easily implemented variable-period structure for quantization error reduction is proposed. Although this variable-period strategy is designed for the inertia identification in this paper, it is also suitable for other situations where speed differential calculation is needed.

In order to symbolically describe the influence of encoder quantization error, a following direct inertia calculation including speed noise is used for further analysis:

$$J = \frac{K_t i_q T_s}{\omega_m\,(k) - \omega_m\,(k-1) + \Delta\omega} \tag{21}$$

in which, $\Delta\omega$ is the noise in the speed feedback signal, and T_s is the calculation period.

Assuming the system is equipped with *N* impulses/revolution encoders and the *M* method is used to acquire the motor speed, the minimum speed measurement resolution can be expressed as

$$E = \frac{2\pi}{NT_{\mathrm{ASR}}}. \tag{22}$$

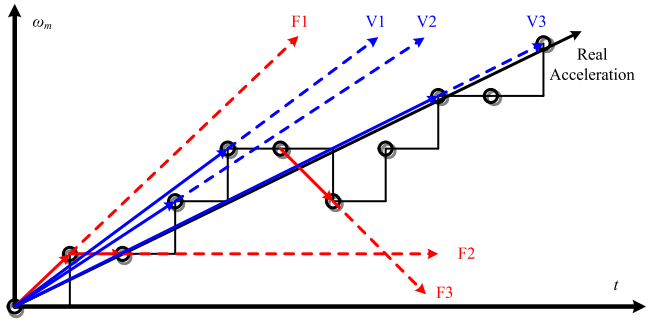

Fig. 4. Comparison of acceleration calculation results.

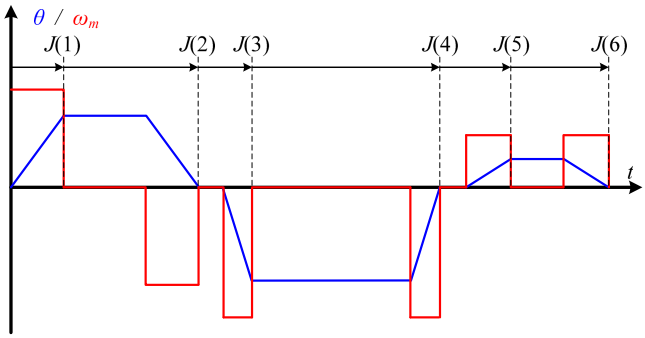

Fig. 5. Position mode periodic inertia update condition redefinition.

The maximum inertia-identification percentage error $\Delta J_{\omega\max}$ can be calculated as (assuming $|\omega_m(k)-\omega_m(k-1)|>E$)

$$\Delta J_{\omega\max}=\max\left\{\left|\frac{\frac{K_t i_q T_s}{\omega_m(k)-\omega_m(k-1)}-\frac{K_t i_q T_s}{\omega_m(k)-\omega_m(k-1)\pm E}}{\frac{K_t i_q T_s}{\omega_m(k)-\omega_m(k-1)}}\right|\right\}$$

$$=\max\left\{\left|1-\frac{d\omega_m/dt}{d\omega_m/dt+E/T_s}\right|,\left|1-\frac{d\omega_m/dt}{d\omega_m/dt-E/T_s}\right|\right\}. \quad (23)$$

The minimum acceleration to meet the predetermined $\Delta J_{\omega\max}$ can be calculated as

$$\left|\frac{d\omega_m}{dt}\right|_{\min}\geq\max\left\{\frac{(1-\Delta J_{\omega\max})E}{\Delta J_{\omega\max}T_s},\frac{(1+\Delta J_{\omega\max})E}{\Delta J_{\omega\max}T_s}\right\}$$

$$=\frac{(1+\Delta J_{\omega\max})E}{\Delta J_{\omega\max}T_s}=\frac{2\pi(1+\Delta J_{\omega\max})}{\Delta J_{\omega\max}NT_sT_{\mathrm{ASR}}}. \quad (24)$$

According to (24), the minimum acceleration is inversely proportional to the calculation period T_s. Thus, adjustment of T_s based on the actual acceleration of the system can expand the application range of inertia identification. Multiplying both sides of (24) by T_s, then, the calculation period criterion of the variable-period inertia-identification strategy can be given as

$$|\omega_m(k)-\omega_m(k-i)|_{\min}\geq\frac{2\pi(1+\Delta J_{\omega\max})}{\Delta J_{\omega\max}NT_{\mathrm{ASR}}}. \quad (25)$$

Thus, the variable-period acceleration input of inertia identification can be given as

$$\frac{d\omega_m}{dt}=\frac{\omega_m(k)-\omega_m(k-i)}{iT_s} \quad (26)$$

in which i is the first time the speed differential result meets the requirement of (25).

The acceleration calculation results of the fixed period strategy and the variable-period strategy when acceleration is slower than minimum speed measurement resolution are shown in Fig. 4. Black hollow circles "O" represent measured speed. Red lines (line "F1," "F2," and "F3") show three types of acceleration results with fixed calculation periods. Blue lines (line "V1," "V2," and "V3") indicate three types of acceleration results from variable calculation periods. The longest black line "R1" represents the real acceleration. Results show that, when the calculation period is fixed, because only three kinds of potential acceleration results exist, the measured accelerations are far from the actual result. Conversely, with the addition of the calculation period criterion (25) and the increase of the speed differential threshold, the acceleration estimation error can be reduced significantly.

Because the calculation period is changed, the i_q input is also needed to be modified as

$$i_q=\sum_{n=k-i+1}^{k}i_q(n)/i. \quad (27)$$

To sum up, the noise model that is built in this part is used to analyze the proportion of the encoder quantization error in the received acceleration signal. Based on this model, the calculation period criterion of the variable-period inertia-identification strategy (25) is just a simplified guide for choosing the speed differential threshold from the perspective of signal processing. Rather than filters, this method can achieve noise reduction simply, without increasing the signal phase lag that occurs when speed varies quickly. In addition, considering that working at a constant speed is also possible for a motor, a time threshold $T_{\lim}$ is set up. If waiting time is larger than $T_{\lim}$, this algorithm will skip condition (25) and calculate motor acceleration from acquired data.

B. Periodic Inertia Update Condition Redefinition

The prerequisite of traditional inertia identification is that motor speed should be periodic. However, this condition cannot be satisfied in most industrial applications. Thus, to make this kind of inertia-identification strategy more applicable, a modification of precondition (6) is needed. Most servo systems work in position-regulation mode. In contrast with speed mode, reciprocating motion and frequent start–stop movement are more common in position control. Thus, zero-speed or zero-cross point appears frequently in these systems. Hence, changing the calculation condition of (8) from fixed period to "speed equal to zero" is a better choice in position regulation, which can then be expressed as

$$\omega_m(k)=\omega_m(k-i^*)=0,\quad \frac{d\omega_m}{dt}\not\equiv 0 \quad (28)$$

in which i^* is the last time the speed was equal to zero.

Fig. 5 is the sketch of the redefined inertia update mode. Although the update period is variable, the new condition (28)

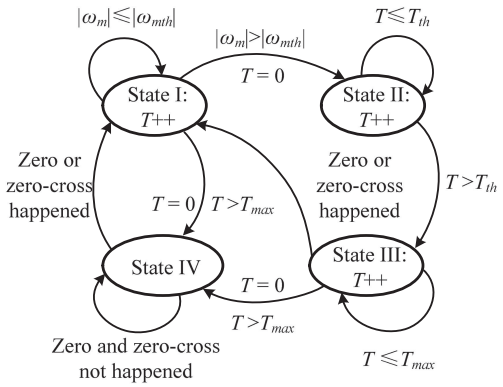

Fig. 6. Additional judging condition states of position mode periodic inertia update condition redefinition.

can also guarantee the validity of (7) as well as the old condition (6). Moreover, compared with (6), (28) has a larger application range in servo position regulation.

However, this condition is still not sufficiently comprehensive. The range of speed variation and the length of the integration period are closely related to identification precision, and the data register will possibly overflow if the integration time is too long. Thus, four additional judging condition states are added.

State I: Preset a speed threshold ω_{mth} and count the past time in State I. If motor speed is larger than ω_{mth}, move to State II. ω_{mth} can guarantee that the variation range of speed is wide enough for inertia identification; if the value in the time register is larger than the maximum time threshold $T_{\max}$, clear up the time register and move to State IV. The setup of $T_{\max}$ can avoid the spill of the integration and the time register.

State II: Count the past time in State II. If the value in time register T is larger than the time threshold T_{th}, move to State III and clear up the time register. T_{th} can guarantee the calculation period is long enough for inertia identification.

State III: Count the past time in State III. If the zero speed or zero-cross speed appears, update observed inertia, clear up the time register, and move back to State I; if the value in the time register is larger than the maximum time threshold $T_{\max}$, clear up the time register and move to State IV.

State IV: Wait until the first time that a new zero speed or zero-cross speed appears. Move back to State I.

The state transition diagram of additional judging conditions is shown in Fig. 6.

Overall, the variable-period strategy and the modified update condition can expand the application range of the conventional inertia identification and make this classic algorithm work accurately.

IV. Constraint Analysis of Expected Controller Maximum Bandwidth

Using the variable-period strategy, a better inertia-identification performance can be achieved. The next step is to obtain suitable controller parameters based on the observed inertia. Although the relationship between inertia and control gain without saturation and limitation has been described by classic parameter-tuning formulas (15) and (19), the expected system bandwidth ω_{sc} and ω_{pc}, as important users' input values, still lack a setting standard or at least tuning guidance. In fact, there is an inseparable relationship between moment inertia and the maximum bandwidth of a system, and the upper boundary of expected system bandwidth still needs further discussion. In this part, to avoid the unlimited increase of controller gain and to drive the servo motor stably, four constraint models, including the physical limit constraint of the speed loop bandwidth, the linear control constraint of the speed loop bandwidth, the physical limit constraint of the position loop bandwidth, and the hardware maximum bandwidth are determined by taking the inertia, controller saturation, and hardware capacity into consideration.

A. Physical Limit Constraint of the Speed Loop Bandwidth

The physical relationship between T_e, acceleration $d\omega_m/dt$ and i_q can be expressed as (without load torque)

$$T_e = K_T i_q = J\frac{d\omega_m}{dt}. \tag{29}$$

Assuming there is a sinusoidal speed reference, and its frequency is ω, and its amplitude is $x_1 A_{\mathrm{std}}$ (where A_{std} is the nominal speed of the motor, and x_1 is the amplitude factor), this reference can be given as

$$\omega_{m\,\mathrm{ref}} = x_1 A_{\mathrm{std}} \sin(\omega t). \tag{30}$$

Substituting (30) into (29), and taking the amplitude attenuation in (13) into consideration, the physical limit constraint of the speed loop bandwidth can be calculated as

$$\omega_{\mathrm{sc}} = \frac{\sqrt{2}K_T}{x_1 A_{\mathrm{std}} J} i_q \le \frac{\sqrt{2}K_T}{x_1 A_{\mathrm{std}} J} i_{q\,\max} \tag{31}$$

in which $i_{q\max}$ is the output limit of the speed controller. An ω_{sc} which does not satisfy (31) is unreachable due to saturation nonlinearity.

B. Linear Control Constraint of Speed Loop Bandwidth

Assuming that the motor speed feedback ω_m from the speed reference (30) is expressed as follows (where x_2 is the amplitude attenuation factor, $0 < x_1 < x_2$, θ_d is the angle delay)

$$\omega_m = x_2 A_{\mathrm{std}} \sin(\omega t + \theta_d). \tag{32}$$

Then, according to (30) and (32), the input of the speed controller $\Delta\omega_m$ can be expressed as

$$\Delta\omega_m = \omega_{m\,\mathrm{ref}} - \omega_{\mathrm{mfbk}} = x_1 A_{\mathrm{std}} \sin(\omega t) - x_2 A_{\mathrm{std}} \sin(\omega t + \theta_d). \tag{33}$$

In the condition of (33), the maximum input $\Delta\omega_{\max}$ can be calculated as

$$\Delta\omega_{m\,\max} = \sqrt{(x_1 A_{\mathrm{std}})^2 + (x_2 A_{\mathrm{std}})^2 - 2x_1 x_2 A_{\mathrm{std}}^2 \cos\theta_d}. \tag{34}$$

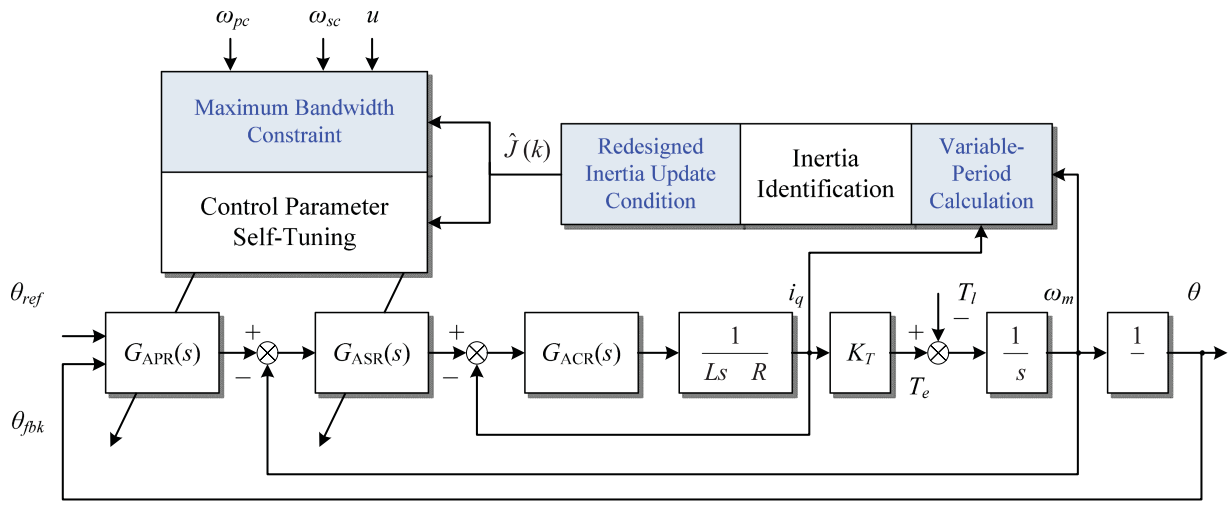

Fig. 7. Structure of improved controller parameter self-tuning via inertia identification.

The maximum output of the speed controller (ignoring the influence from K_{sidis}) can be given as

$$K_{\mathrm{spdis}}\Delta\omega_{m\,\max} = i_q \le i_{q\,\max}. \tag{35}$$

By substituting (16) and (34) into (35), and ignoring the influence from the smaller items that include T_{ASR}, the linear control constraint of the speed loop bandwidth can be calculated as

$$\omega_{\mathrm{sc}} \le \frac{i_{q\,\max}u_{\mathrm{fix}}K_T}{J\sqrt{(x_1A_{\mathrm{std}})^2+(x_2A_{\mathrm{std}})^2-2x_1x_2A_{\mathrm{std}}^2\cos\theta_d}} \tag{36}$$

in which x_2 and θ_d are selected by a variety of methods. There are two types of combinations for reference. The first one is $x_2 = x_1$ and $\theta_d = -\pi$, which can guarantee that the speed loop is never saturated in the stable state. Another one is $x_2 = 0.707x_1$ and $\theta_d = -\pi/2$. In this condition, a stable system can work in a linear state within expected bandwidth. Because the first one is too strict, the second type is used in this paper.

C. Physical Limit Constraint of Position Loop Bandwidth

In most servo systems, trajectory planning exists to avoid the saturation of the position loop. Thus, the output limit of the position loop is ignored in this part. The physical relation among $d^2\theta/dt^2$ and i_q can be expressed as

$$K_T i_q = J\frac{d^2\theta}{dt^2}. \tag{37}$$

Similar to the analysis of the speed loop, assuming there is a sinusoidal position reference, and its frequency is ω while amplitude is x_3, the position reference can be given as

$$\theta_{\mathrm{ref}} = x_3\sin(\omega t). \tag{38}$$

Substituting (38) into (37), and taking the amplitude attenuation of ω_{pc} into consideration, the physical limit constraint of the position loop bandwidth can be calculated as

$$\omega_{\mathrm{pc}} = \sqrt{\sqrt{2}K_T i_q/(x_3J)} \le \sqrt{\sqrt{2}K_T i_{q\,\max}/(x_3J)}. \tag{39}$$

D. Hardware Maximum Bandwidth

In fact, the physical limit constraint also exists in the current loop. This constraint comes from the hardware capacity. For surface permanent magnet synchronous motors, the relation among bus voltage u_{dc}, phase resistance R, the number of poles p, the flux linkage of the magnet ψ_f, and phase inductance L without overmodulation can be given as

$$\frac{\sqrt{3}u_{\mathrm{dc}}}{3} = Ri_q + L\frac{di_q}{dt} + p\omega_m\psi_f. \tag{40}$$

Assuming there is a sinusoidal current in the q-axis, and its frequency is ω and amplitude is $i_{q\max}$, then making a conservative estimate, the physical limit constraint of the current loop following performance can be calculated as

$$\omega = \frac{\sqrt{3}u_{\mathrm{dc}}/3 - Ri_{q\,\max}\sin(\omega t) - p\,\omega_m\psi_f}{Li_{q\,\max}\cos(\omega t)}$$

$$\Rightarrow \omega \le \frac{\sqrt{3}u_{\mathrm{dc}} - 3Ri_{q\,\max} - 3pA_{\mathrm{std}}\psi_f}{3Li_{q\,\max}}. \tag{41}$$

Equation (41) is the hardware maximum unsaturation bandwidth of the position and speed loops. Keeping the expected system bandwidth within this range can guarantee that the system has the possibility to work in the linear control state in most operating conditions ($|\omega_m| < |A_{\mathrm{std}}|$).

In order to reduce the online computation burden, we set q_1, q_2, q_3, q_4 as pretreatment coefficients. They can be given as

$$\begin{cases} q_1 = \sqrt{2}K_T i_{q\max}/(x_1A_{\mathrm{std}}) \\ q_2 = i_{q\,\max}u_{\mathrm{fix}}K_T/ \\ \qquad \sqrt{(x_1A_{\mathrm{std}})^2+(x_2A_{\mathrm{std}})^2-2x_1x_2A_{\mathrm{std}}^2\cos\theta_d} \\ q_3 = \sqrt{2}K_T i_{q\,\max}/x_3 \\ q_4 = \left(\sqrt{3}u_{\mathrm{dc}} - 3Ri_{q\,\max} - 3pA_{\mathrm{std}}\psi_f\right)/(3Li_{q\,\max}). \end{cases} \tag{42}$$

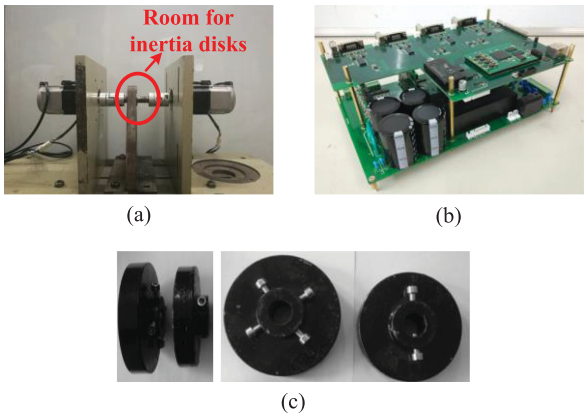

Fig. 8. Experimental setup. (a) Platform. (b) Multiaxis controller. (c) Inertia disks.

TABLE I
MAIN PARAMETERS OF THE SERVO DRIVE SYSTEM

Parameter	value
Motor Power P_N	750 W
Nominal Torque T_{eN}	2.39 N·m
Nominal Speed ω_N	3000 r/min
Nominal Current i_{qN}	5×1.414 A
Maximum Current $i_{q\max}$	5×1.414×3 A
Bus Voltage U_{dc}	300 V
Poles p	4
Phase Resistance R	0.8 Ω
Phase Inductance L	2.45 mH
Flux Linkage of Magnet ψ_f	0.05633 Wb
Inertia of drive motor J_m	1.3e-4 kg·m^2
Inertia of Load I J_1	1.30351e-3 kg·m^2
Inertia of Load II J_2	6.2631e-4 kg·m^2
Encoder Pulses	2^17 lines
Sampling Period T_{APR} & T_{ASR}	2.5e-4 s

Then, the upper limits of the expected closed-loop bandwidth of the speed and position controllers can be expressed as

$$\begin{cases} \omega_{\mathrm{sc}} \le \min\{q_1/J, \quad q_2/J, \quad q_4\} \\ \omega_{\mathrm{pc}} \le \min\left\{\sqrt{q_3/J}, \quad \omega_{\mathrm{sc}}\right\}. \end{cases} \tag{43}$$

To sum up, since the controller's output saturation has not been considered by the conventional controller parameter tuning, actually, (43) is a kind of compromise to ensure the normal operation of the system (as it works in a linear state) under different applications (in which the inertia of the system can be changed over a large range). Moreover, because commercial universal servos have variable applications, the delay of the system caused by discrete control, mechanical damping, communication, and measurement is usually hard to accurately model in advance. Thus, the real phase margin of the system cannot be described by the conventional simplified model, and systems still have the possibility to be unstable when controller gain is too large. In this situation, a suitable maximum bandwidth constraint can be helpful to make systems work in a moderate state. The boundary factors x_1 and x_3 can be selected based on the determined hardware maximum bandwidth or by implementing several simple offline tests in certain applications.

Finally, by utilizing a variable-period strategy and adding maximum bandwidth constraint, two main parts of the controller parameter self-tuning method, inertia identification and parameter calculation, have been modified. The structure of the improved controller parameter self-tuning via inertia identification can be shown in Fig. 7, and the proposed three improvements are highlighted in blue.

TABLE II
MAIN PARAMETERS OF THE CONTROLLER

Parameter	value
ω_{pc}	2π×20 rad/s
ω_{sc}	2π×200 rad/s
u	5.67
x_1	0.05
x_2	0.05×0.707
θ_d	-π/2 rad
x_3	1.5×2π rad
$\Delta J_{\omega\max}$	10%
T_{lim}	0.1 s
ω_{mth}	100 rpm
T_{th}	0.025 s
T_{max}	5 s

V. EXPERIMENTAL RESULTS

The experiment platform is shown in Fig. 8. Two TAMAGAWA TS4614N7680 servo motors are used as the driver and the load, respectively. In addition, two different inertia disks are used to adjust the total inertia of the platform. The inertia identification and controller parameter self-tuning algorithm in Fig. 7 are built into the multiaxis controller.

The control chip of the multiaxis controller is a Xilinx Zynq series system on chip (SoC), which integrates advanced reduced instruction set computer machines (ARM, two Cortex-A9s but only one is used) and a field-programmable gate array (FPGA) into one chip. The FPGA is responsible for the current control and one ARM is used to deal with the position and speed regulation. In addition, to record experimental data, the random access memory of the Zynq was extended to 1 GB by adding an external memory chip. The control of both the drive motor and the load motor is handled by a single controller. The detailed parameters of the servo drive system

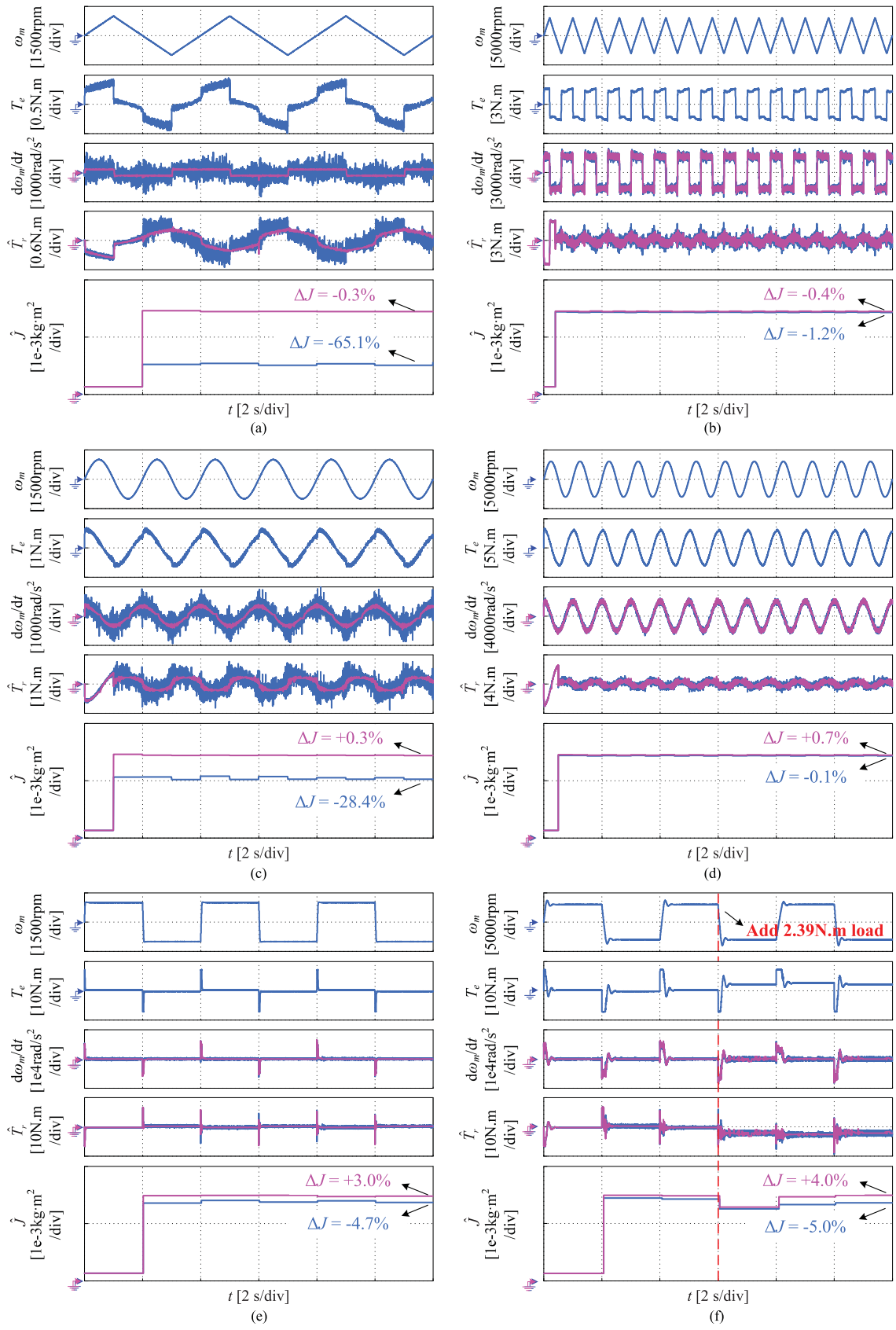

Fig. 9. Comparison of inertia-identification results under different situations and accelerations, in which the blue line represents the fixed-period method and the purple line represents the proposed variable-period method. (a) $|d\omega_m/dt| = 105.72$ rad/s^2 = 1000 r/min/s. (b) $|d\omega_m/dt| = 1570.80$ rad/s^2 = 15 000 r/min/s. (c) $\omega_{\mathrm{m\,ref}} = 1000$ r/min $\times$ sin(πt). (d) $\omega_{\mathrm{m\,ref}} = 3000$ r/min $\times$ sin(2πt). (e) 1000 r/min step. (f) 3000 r/min step, with a 2.39 N·m switching load.

are presented in Table I, and the main parameters of the proposed algorithm are listed in Table II. As reference values, the load inertia I J_1 and II J_2 are measured by high-precision offline inertia identification. Additionally, taking the antiwindup of the PI controllers into consideration, the incremental structure is used in the current controller while the integration-weakening PI regulation strategy is applied in the speed controller.

A. Variable Calculation Period Strategy

Three types of speed references including triangle, sine, and step are used to verify the noise-reduction performance of the variable-period speed differential strategy. Sets of typical results are shown in Fig. 9. Motor speed ω_m, electrical torque T_e, acceleration $d\omega_m/dt$, equivalent disturbance torque $\hat{T}_r(t)$, and observed inertia $\hat{J}$ are recorded. The classic fixed-period method and the proposed variable-period method are running simultaneously, while the system is tracking speed reference (in this experiment, the speed controller is roughly manually adjusted). The factor λ–related low-pass filter cutoff frequency of both methods is 200 Hz. Except for ω_m and T_e, the blue lines of other data represent the fixed-period method, while the purple lines represent the variable-period method. Fig. 9(a) and (b) shows results under the triangular speed reference, but $|d\omega_m/dt|$ of Fig. 9(a) is lower than that of (b). Experimental results show that, although the inertia-identification accuracy of the fixed-period method decreases with the slowing of the acceleration, the proposed variable-period strategy can still generate a high-precision inertia result when speed changes slowly. Fig. 9(c) and (d) shows results both under the sinusoidal speed reference. Similar to Fig. 9(a) and (b), the proposed variable-period method has better performance under slow acceleration. Fig. 9(e) and (f) proves both methods are still useful under square wave speed, in which the speed variation time is relatively short. In addition, a constant 2.39 N·m load is added by a load-side motor in the 6 s of Fig. 9(f). Although this disturbance causes a slight fluctuation of observed inertia, the estimation result is ultimately restored to the exact value.

In order to visually reflect the advantage of the variable-period strategy, an experimental results summary (not only the data in Fig. 9, but also other remaining experimental results) showing the relationship between inertia-identification error and acceleration is made in Fig. 10. Because of the existence of the low-pass filter in the speed measurement and disturbance observer, and because the constraint (23) is a maximum error function, the theoretical error bound is higher than the experimental fixed-period inertia-identification error, but they have the same tendency. Compared with the fixed-period method, the proposed variable-period speed differential calculation method has better noise-reduction capacity and can achieve higher precise inertia estimation in low acceleration situations.

B. Redesigned Periodic Inertia Update Condition

The comparison of inertia-identification results with different modes and references is shown in Fig. 11. The inertia update

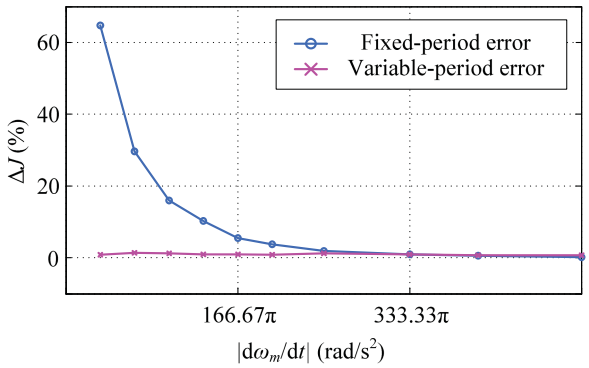

Fig. 10. Relationship between inertia-identification error and acceleration.

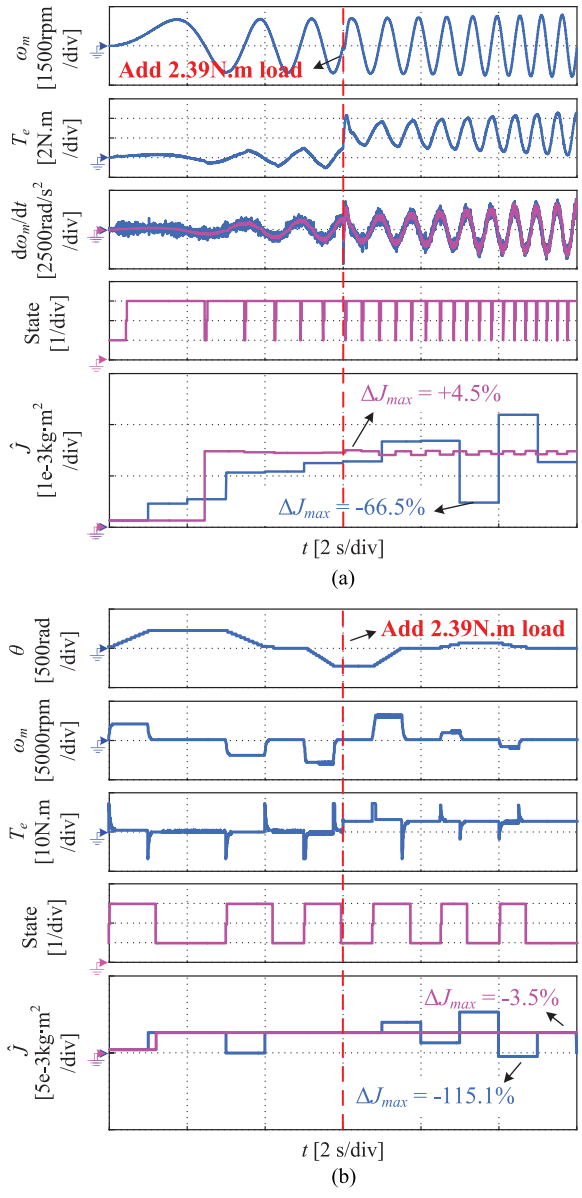

Fig. 11. Comparison of inertia-identification results with different modes and references, in which the blue line represents fixed-period method and the purple line represents proposed variable-period method. (a) Chirp speed reference. (b) Irregular position reference.

period of the conventional method is set as 1 s, and a 2.39 N·m load is added in the 6th second. Both speed and position control modes are used to test the performance of the proposed zero or zero-cross inertia update condition. Moreover, the additional judging condition state of the proposed method is also recorded. Fig. 11(a) and (b) shows the inertia-identification results of different methods under chirp speed reference and irregular position reference. Because the period of the speed command is not fixed, the precondition (6) of the traditional method with a fixed inertia update period is not valid anymore. Thus, the observed inertia from the conventional method varies over a wide range. On other hand, owing to the redesigned self-adaptive inertia update condition, the proposed method has more stable and better identification performance.

C. Inertia Identification-Based Controller Self-Tuning Method With Maximum Expected Bandwidth Constraints

According to the analysis in Section IV and the predetermined parameters in Table II, the bandwidth constraints are shown in Fig. 12 (where J_x is the load inertia). In order to best guarantee that the system works in the linear state and avoid the unlimited increase of controller gain, these constraints are used to modify the expected bandwidth under different types of load inertia.

As an example, Fig. 13 is the system performance under speed mode and position mode after parameter tuning but without maximum bandwidth. Since the gain of the controller is too large, severe speed oscillation and position vibration appear. Thus, the maximum expected bandwidth constraint is necessary. When the maximum bandwidth constraint is adopted, the system can evaluate the validity of the users' input based on the observed inertia, and use the upper limitation to fix the expected bandwidth.

The online parameter self-tuning performances with the maximum bandwidth constraint under speed- (with square wave reference and triangular reference) and position-regulation mode are shown in Figs. 14–Fig. 16, respectively. Two types of load inertia, inertia I and inertia II, are tested to verify the performance of the proposed algorithm. In order to make the tuning process smoother, a simple filter is added before the inertia-identification output. The output inertia is the average value of the last used inertia and the newly acquired estimated inertia.

$$J_u(k) = (J_u(k-1) + J_o(k))/2, \quad J_u(0) = J_o(0) = J_m \tag{44}$$

in which J_u is the used inertia for controller parameter self-tuning, J_o is the observed inertia, and J_m is the inertia of motor itself.

In Fig. 14(a) and (b), the overshoot of the motor speed decreases from 177 r/min to 29 r/min and from 157 r/min to 42 r/min, respectively. Moreover, in Fig. 15(a) and (b), the distortion of motor speed response under triangular speed reference is also decreased after parameter modification. Therefore, if zero speed or zero-cross speed exists, the proposed online controller parameter self-tuning method does not require that the system work in a certain mode or with predetermined reference (such as a step signal). Furthermore, in Fig. 16(a) and (b), when the system works in the position mode, in accordance with the

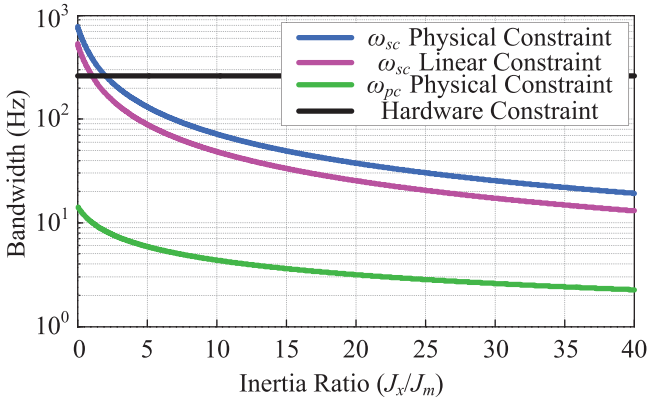

Fig. 12. Maximum expected bandwidth constraints.

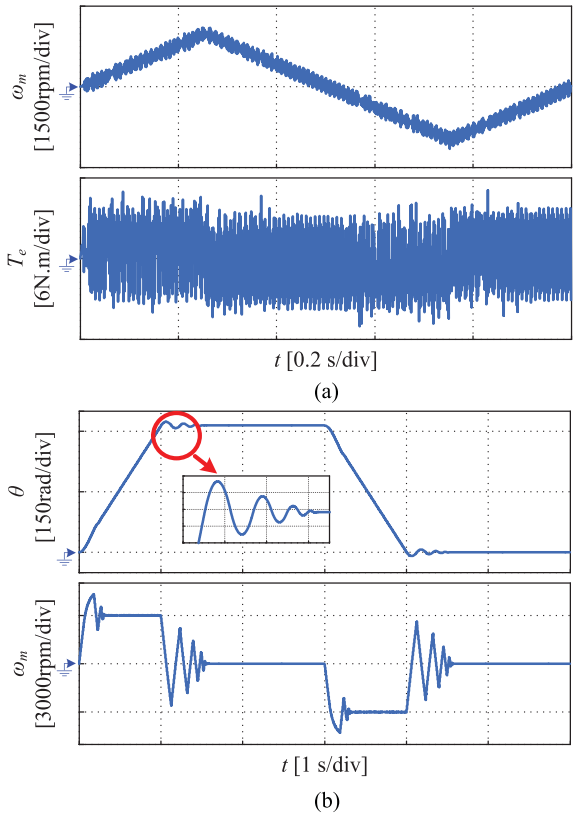

Fig. 13. Parameter self-tuning performance without maximum bandwidth constraints in the system with inertia I. (a) $\omega_{\rm sc} = 200$ Hz. (b) $\omega_{\rm pc} = 40$ Hz.

process of inertia identification and parameter self-tuning, not only do the unacceptable overshoots of the position feedback (14 4579 pulses and 45 612 pulses) disappear, but the oscillation and vibration phenomena in the start-up and stop stage also have been suppressed successfully. In addition, the online inertia identification is still working steadily, and highly accurate inertia observation results are obtained ($|\Delta J| < 6\%$) under both the speed- and position-regulation modes. As for stability, it is worth mentioning that, in contrast with the severe speed oscillation and position vibration in Fig. 13, the damped oscillation of speed and the overshoot of position in Figs. 14–Fig. 16 are caused by the mismatch of the initial inertia and actual inertia. In detail, the speed controller gain is very small and the position

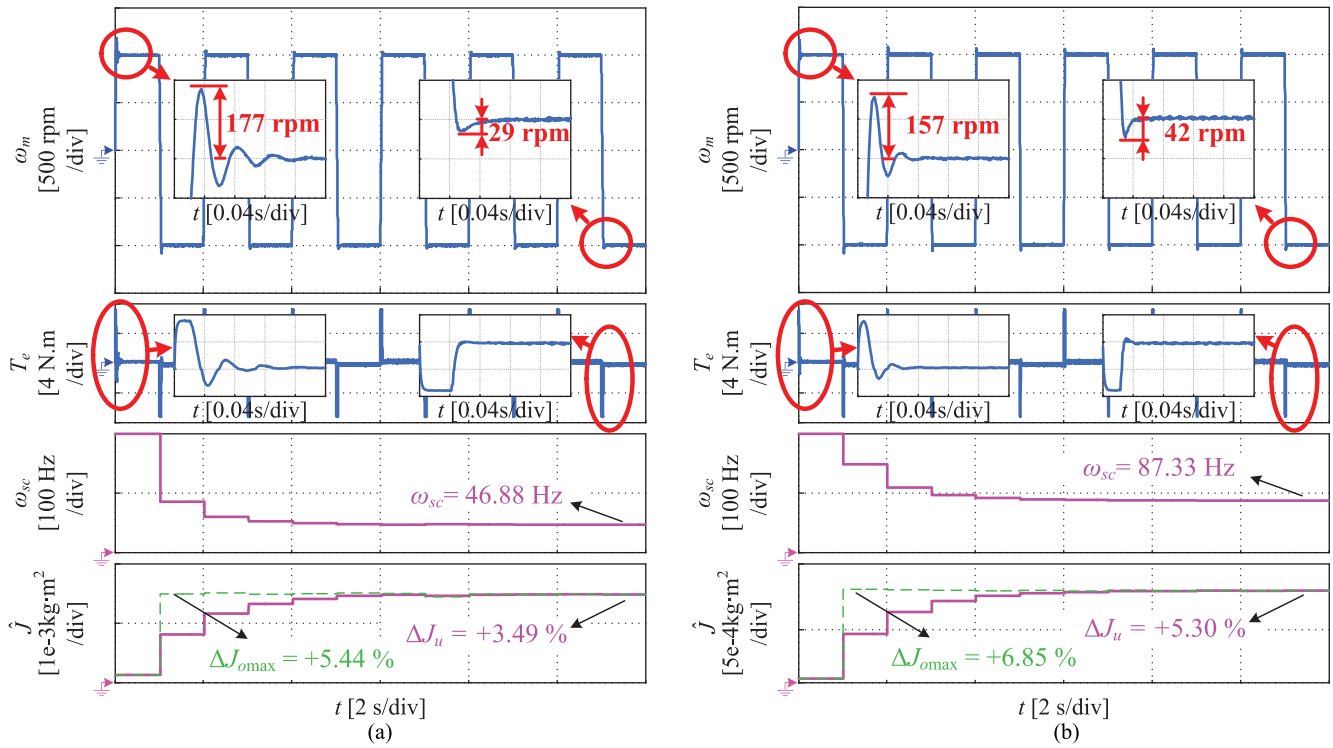

Fig. 14. Online parameter self-tuning performance with maximum bandwidth constraint under square-wave speed reference. (a) System with Inertia I. (b) System with Inertia II.

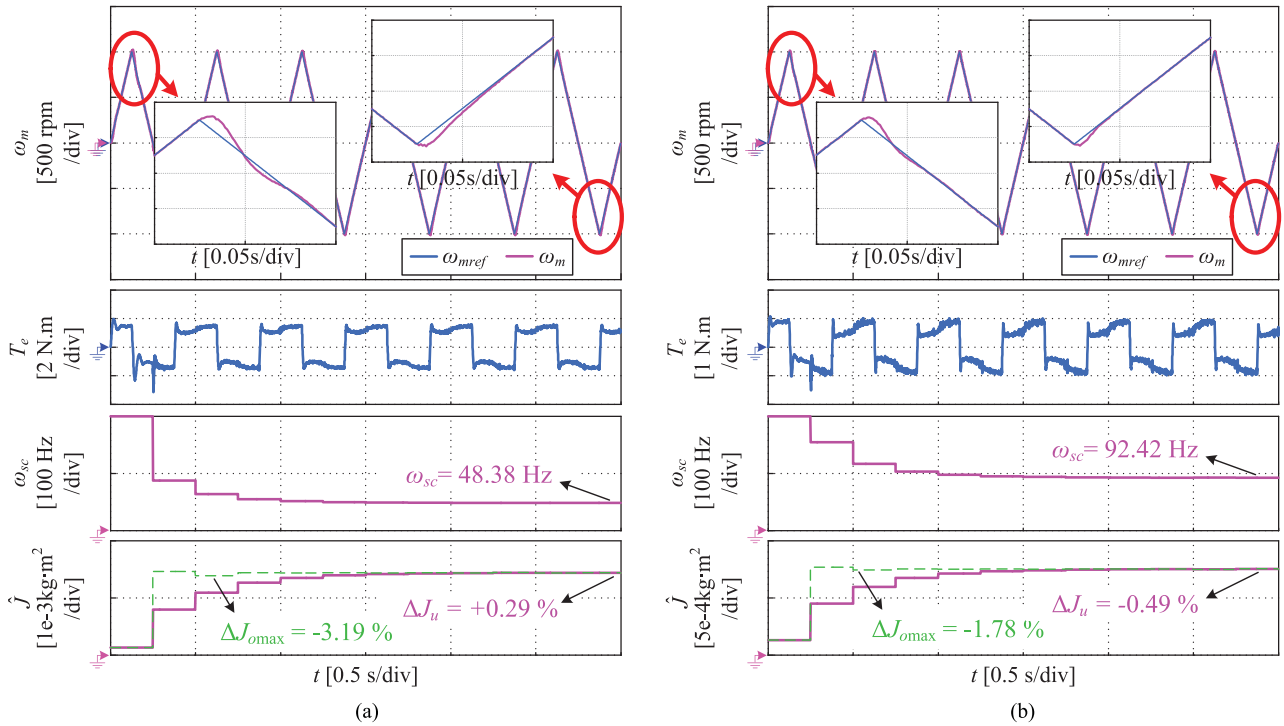

Fig. 15. Online parameter self-tuning performance with maximum bandwidth constraint under triangular speed reference. (a) System with Inertia I. (b) System with Inertia II.

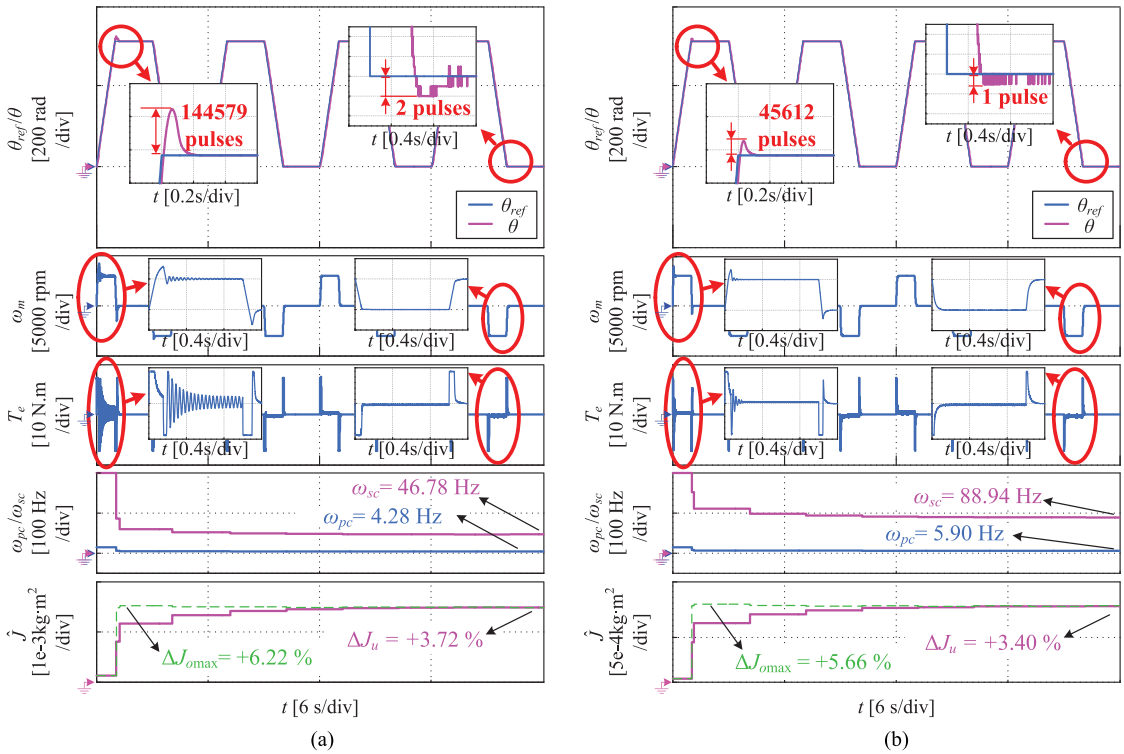

Fig. 16. Online parameter self-tuning performance with maximum bandwidth constraint under position mode. (a) System with Inertia I. (b) System with Inertia II.

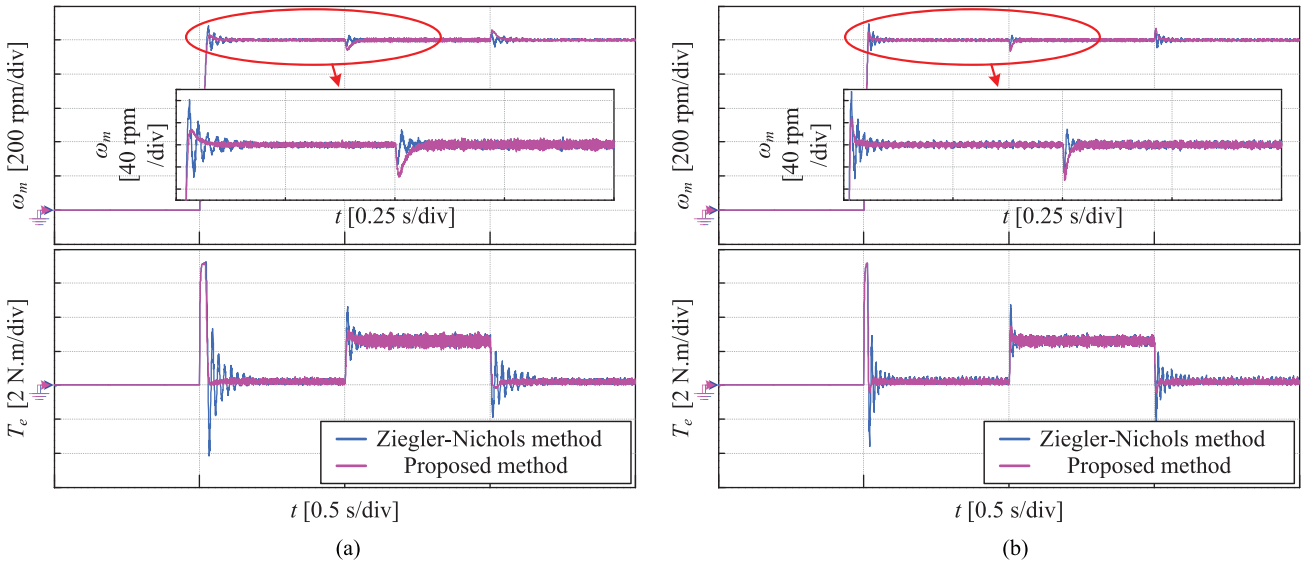

Fig. 17. Controller performance of the classic Ziegler−Nichols method and tuning result of the proposed method. (a) System with Inertia I. (b) System with Inertia II.

controller gain is relatively large, but the entire system is still in a stable state owing to the existence of the maximum bandwidth constraints (users' unreasonable expected system bandwidth input can be self-corrected). Moreover, if the first and the second prerequisites of this inertia estimation method are still valid, in Figs. 14–Fig. 16, although the system does not reach the steady state at the beginning of the controller parameter self-tuning process (overshoot and oscillation exist), the observed inertia results, which are shown by the green dotted lines, are still relatively accurate. The filter (44) between the observed inertia and the input inertia for parameter self-tuning is used to reduce the influence of the controller output mutation caused by the controller parameter adjustment.

Finally, a set of comparison results (PI controller, speed mode) between tuning results of the widely used Ziegler–Nichols method and the proposed method are shown in Fig. 17. It can be seen that the controller tuned by the proposed method has smaller overshoot and lacks damped oscillation. When a

2.39 N·m (nominal torque) switching load is added, although the speed drop and recovery time of the Ziegler–Nichols method are relatively smaller, the performance of the proposed method is smoother and vibrationless (both motor speed and torque response).

To sum up, because of the maximum bandwidth constraint, the online controller parameter self-tuning method in this paper can avoid the frequent saturation of the controller and keep the system work smoothly in most normal situations. Although the tuning result might be not optimal or slightly conservative, it can provide reference or initial values for further modification by manual setting or rule-based controller parameter tuning. In particular, the proposed variable-period inertia-identification method can be applied more successfully in those reciprocating motion situations with lower angular acceleration. Additionally, if the entire system is stable and the first and the second prerequisites of this inertia estimation method are still valid (it is also one of the reasons to use a slightly conservative parameter self-tuning strategy with the maximum bandwidth), although the system does not reach the steady state or track the velocity command well, the improved method still can obtain a relatively highly accurate inertia estimation result by adaptively judging the timing for the inertia update.

VI. Conclusion

In this paper, based on the detailed analysis of the conventional inertia-identification and model-based controller parameter self-tuning methods, three targeted modified strategies are proposed. First, a variable-period speed differential calculation strategy is presented to reduce the measurement noise caused by the encoder-quantization error. Then, a zero or zero-cross speed condition is adopted to replace the traditional fixed periodic inertia update mode. In addition, several judging states are added to guarantee the inertia-identification accuracy and avoid registry overflows. Owing to the variable-period structure of both the speed differential calculation and the inertia update, the improved inertia-identification method can work stably and precisely in more complex and demanding patterns. As for the controller parameter self-tuning method, in order to acquire a suitable upper limit of expected controller bandwidth under different inertia, a maximum bandwidth model is built by taking constraints from controller saturation nonlinearity and hardware capacity into consideration. The effectiveness and merits of the modified algorithm are verified in different types of experiments and data analyses. Mechanical friction identification and compensation, and combining the model-based and rule-based controller self-tuning method for better control performance are the future research emphases.

References

[1] R. Tami, D. Boutat, G. Zheng, F. Kratz, and R. E. Gouri, "Rotor speed, load torque, and parameters estimations of a permanent magnet synchronous motor using extended observer forms," *IET Control Theory Appl.*, vol. 11, no. 9, pp. 1485–1492, May 2017.

[2] W. Huang, C. Liu, P. Hsu, and S. Yeh, "Precision control and compensation of servomotors and machine tools via the disturbance observer," *IEEE Trans. Ind. Electron.*, vol. 57, no. 1, pp. 420–429, Jan. 2010.

[3] D. Lee, and J. Ahn, "Dual speed control scheme of servo drive system for a nonlinear friction compensation," *IEEE Trans. Power Electron.*, vol. 23, no. 2, pp. 959–965, Mar. 2008.

[4] S. Kim, "Moment of inertia and friction torque coefficient identification in a servo drive system," *IEEE Trans. Ind. Electron.*, vol. 66, no. 1, pp. 60–70, Jan. 2019.

[5] J. Yao, Z. Jiao, and D. Ma, "Adaptive robust control of dc motors with extended state observer," *IEEE Trans. Ind. Electron.*, vol. 61, no. 7, pp. 3630–3637, Jul. 2014.

[6] F. Lin, P. Chou, C. Chen, and Y. Lin, "DSP-based cross-coupled synchronous control for dual linear motors via intelligent complementary sliding mode control," *IEEE Trans. Ind. Electron.*, vol. 59, no. 2, pp. 1061–1073, Feb. 2012.

[7] T. Kweon, and D. Hyun, "High-performance speed control of electric machine using low-precision shaft encoder," *IEEE Trans. Power Electron.*, vol. 14, no. 5, pp. 838–849, Sep. 1999.

[8] J. Jung, V. Q. Leu, T. D. Do, E. Kim, and H. H. Choi, "Adaptive PID speed control design for permanent magnet synchronous motor drives," *IEEE Trans. Power Electron.*, vol. 30, no. 2, pp. 900–908, Feb. 2015.

[9] V. Q. Leu, H. H. Choi, and J. W. Jung, "Fuzzy sliding mode speed controller for PM synchronous motors with a load torque observer," *IEEE Trans. Power Electron.*, vol. 27, no. 3, pp. 1530–1539, Mar. 2012.

[10] K. Y. Cheng and Y. Y. Tzou, "Fuzzy optimization techniques applied to the design of a digital PMSM servo drive," *IEEE Trans. Power Electron.*, vol. 19, no. 4, pp. 1085–1099, Jul. 2004.

[11] T. D. Do, S. Kwak, H. H. Choi, and J. W. Jung, "Suboptimal control scheme design for interior permanent magnet synchronous motors: An SDRE-based approach," *IEEE Trans. Power Electron.*, vol. 29, no. 6, pp. 3020–3031, Jun. 2014.

[12] F. J. Lin, Y. C. Hung, J. C. Hwang, and M. T. Tsai, "Fault-tolerant control of a six-phase motor drive system using a Takagi–Sugeno–Kang type fuzzy neural network with asymmetric membership function," *IEEE Trans. Power Electron.*, vol. 28, no. 7, pp. 3557–3572, Jul. 2013.

[13] R. Wai, "Total sliding-mode controller for PM synchronous servo motor drive using recurrent fuzzy neural network," *IEEE Trans. Ind. Electron.*, vol. 48, no. 5, pp. 926–944, Oct. 2001.

[14] S. Li and Z. Liu, "Adaptive speed control for permanent-magnet synchronous motor system with variations of load inertia," *IEEE Trans. Ind. Electron.*, vol. 56, no. 8, pp. 3050–3059, Aug. 2009.

[15] T. Haidegger, L. Kovács, R. Precup, B. Benyó, Z. Benyó, and S. Preitl, "Simulation and control for telerobots in space medicine," *Acta Astronaut*, vol. 88, no. 1, pp. 390–402, Dec. 2012.

[16] Y. Yam, M. Wong, and P. Baranyi, "Interpolation with function space representation of membership functions," *IEEE Trans. Fuzzy Syst.*, vol. 14, no. 3, pp. 398–411, Jun. 2006.

[17] S. Vrkalovic, E. Lunca, and I. Borlea, "Model-free sliding mode and fuzzy controllers for reverse osmosis desalination plants," *Int. J. Artificial Intell.*, vol. 16, no. 2, pp. 208–222, Oct. 2018.

[18] D. Martãn, B. Caballero, and R. Haber, "Optimal tuning of a networked linear controller using a multi-objective genetic algorithm. Application to a complex electromechanical process," in *Proc. Int. Conf. Innovative Comput. Inf. Control.*, 2008, p. 91, doi: 10.1109/ICICIC.2008.407.

[19] S. Dasgupta, S. N. Mohan, S. K. Sahoo, and S. K. Panda, "Lyapunov function-based current controller to control active and reactive power flow from a renewable energy source to a generalized three-phase microgrid system," *IEEE Trans. Ind. Electron.*, vol. 60, no. 2, pp. 799–813, Feb. 2013.

[20] P. J. Serkies and K. Szabat, "Application of the MPC to the position control of the two-mass drive system," *IEEE Trans. Ind. Electron.*, vol. 60, no. 9, pp. 3679–3688, Sep. 2013.

[21] C. Hsu and Y. Lai, "Novel online optimal bandwidth search and autotuning techniques for servo motor drives," *IEEE Trans. Ind. Appl.*, vol. 53, no. 4, pp. 3635–3642, Jul./Aug. 2017.

[22] M. Tursini, F. Parasiliti, and D. Zhang, "Real-time gain tuning of PI controllers for high-performance PMSM drives," *IEEE Trans. Ind. Appl.*, vol. 38, no. 4, pp. 1018–1026, Jul./Aug. 2002.

[23] K. Liu and Z. Zhu, "Fast determination of moment of inertia of permanent magnet synchronous machine drives for design of speed loop regulator," *IEEE Trans. Control Syst. Technol.*, vol. 25, no. 5, pp. 1816–1824, Sep. 2017.

[24] Y. Lai and M. Ho, "Self-commissioning technique for high bandwidth servo motor drives," in *Proc. Energy Convers. Congr. Expo.*, 2017, pp. 342–349.

[25] L. Niu, D. Xu, M. Yang, X. Gui, and Z. Liu, "On-line inertia identification algorithm for PI parameters optimization in speed loop," *IEEE Trans. Power Electron.*, vol. 30, no. 2, pp. 849–859, Feb. 2015.
[26] A. Lidozzi, V. Serrao, L. Solero, F. Crescimbini, and A. D. Napoli, "Direct tuning strategy for PMSM drives," in *Proc. IEEE Ind. Appl. Soc. Annu. Meeting*, 2008, pp. 1–7.
[27] S.-K. Sul, *Control of Electric Machine Drive Systems*, Hoboken, NJ, USA: Wiley, 2010.
[28] Y. Feng, X. Yu, and F. Han, "High-order terminal sliding-mode observer for parameter estimation of a permanent-magnet synchronous motor," *IEEE Trans. Ind. Electron.*, vol. 60, no. 10, pp. 4272–4280, Oct. 2013.
[29] S. Tafazoli, P. D. Lawrence, and S. E. Salcudean, "Identification of inertial and friction parameters for excavator arms," *IEEE Trans. Robot. Automat.*, vol. 15, no. 5, pp. 966–971, Oct. 1999.
[30] W. Xie, "Sliding-mode-observer-based adaptive control for servo actuator with friction," *IEEE Trans. Ind. Electron.*, vol. 54, no. 3, pp. 1517–1527, Jun. 2007.
[31] Y. Tan, J. Chang, and H. Tan, "Adaptive backstepping control and friction compensation for ac servo with inertia and load uncertainties," *IEEE Trans. Ind. Electron.*, vol. 50, no. 5, pp. 944–952, Oct. 2003.
[32] X. Zhang and Z. Li, "Sliding-mode observer-based mechanical parameter estimation for permanent magnet synchronous motor," *IEEE Trans. Power Electron.*, vol. 31, no. 8, pp. 5732–5745, Aug. 2016.
[33] K. Liu and Z. Q. Zhu, "Mechanical parameter estimation of permanent magnet synchronous machines with aiding from estimation of rotor PM flux linkage," *IEEE Trans. Ind. Appl.*, vol. 51, no. 4, pp. 3115–3125, Jul/Aug. 2015.
[34] F. Andoh, "Inertia identification method based on the product of the integral of torque reference input and motor speed," in *Proc. Int. Council Commercial Arbitration*, 2008, pp. 1151–1158.
[35] M. Calvini, M. Carpita, A. Formentini, and M. Marchesoni, "PSO-based self-commissioning of electrical motor drives," *IEEE Trans. Ind. Electron.*, vol. 62, no. 2, pp. 768–776, Feb. 2015.
[36] Z. Liu, H. Wei, X. Li, K. Liu, and Q. Zhong, "Global identification of electrical and mechanical parameters in PMSM drive based on dynamic self-learning PSO," *IEEE Trans. Power Electron.*, vol. 33, no. 2, pp. 10858–10871, Dec. 2018.
[37] R. Garrido and A. Concha, "Inertia and friction estimation of a velocity-controlled servo using position measurements," *IEEE Trans. Ind. Electron.*, vol. 61, no. 9, pp. 4759–4770, Sep. 2014.
[38] F. Andoh, "Moment of inertia identification using the time average of the product of torque reference input and motor position," *IEEE Trans. Power Electron.*, vol. 22, no. 6, pp. 2534–2542, Nov. 2007.
[39] Y. Yu, Z. Mi, X. Guo, Y. Xu, and T. Zhao, "Low speed control and implementation of permanent magnet synchronous motor for mechanical elastic energy storage device with simultaneous variations of inertia and torque," *IET Electr. Power Appl.*, vol. 10, no. 3, pp. 172–180, Mar. 2016.
[40] K. Lee and F. Blaabjerg, "Robust and stable disturbance observer of servo system for low-speed operation," *IEEE Trans. Ind. Appl.*, vol. 43, no. 3, pp. 627–635, May/Jun. 2007.
[41] S. Yang and Y. Deng, "Observer-based inertial identification for auto-tuning servo motor drives," in *Proc. IEEE Ind. Appl. Soc. Annu. Meeting*, 2005, pp. 968–972.
[42] I. Awaya, Y. Kato, I. Miyake, and M. Ito, "New motion control with inertia identification function using disturbance observer," in *Proc. IEEE Ind. Appl. Soc. Annu. Meeting*, 1992, pp. 77–81.
[43] T. Kwon, S. Sul, H. Nakamura, and K. Tsuruta, "Identification of the mechanical parameters for servo drive," in *Proc. IEEE Ind. Appl. Soc. Annu. Meeting*, 2006, pp. 905–910.
[44] N. Kim, H. Moon, and D. Hyun, "Inertia identification for the speed observer of the low speed control of induction machines," *IEEE Trans. Ind. Appl.*, vol. 32, no. 6, pp. 1371–1379, Nov./Dec. 1996.

Yangyang Chen received the B.S. degree in electrical engineering in 2016 from the Harbin Institute of Technology, Harbin, China, where he is currently working toward the Ph.D. degree in power electronics and electrical drives at the School of Electrical Engineering and Automation.

His current research interests include multi-axis servo systems, mechanical resonance, and control parameter self-tuning strategy.

Ming Yang (M'14–SM'18) received the B.S., M.S., and Ph.D. degrees in electrical engineering from the Harbin Institute of Technology (HIT), Harbin, China, in 2000, 2002 and 2007, respectively.

In 2004, he joined as a Lecturer with the Department of Electrical Engineering, HIT, where he has been a Professor of electrical engineering since 2015. From 2009 to 2012, he was a Postdoctoral Fellow with Shanghai STEP Electric Corporation. He has authored more than 40 technical papers published in journals and conference proceedings. He holds 14 Chinese patents. His current major research interests include permanent magnet synchronous motor servo systems, predictive current control, and mechanical resonance suppression.

Jiang Long received the M.S. degree in power electronics and electrical drives in 2015 from the Harbin University of Science and Technology, Harbin, China. He is currently working toward the Ph.D. degree in power electronics and electrical drives with the School of Electrical Engineering and Automation, Harbin Institute of Technology, Harbin.

His current research interests include permanent magnet synchronous motor servo systems, predictive current control, and parameter identification.

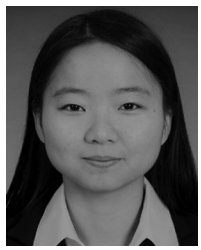

Wanying Qu received the B.S. degree in electrical engineering in 2017 from Harbin Institute of Technology, Harbin, China, where she is currently working toward the M.S. degree in power electronics and electrical drives at the School of Electrical Engineering and Automation.

Her current research interest focuses on permanent magnet synchronous motor servo system and inertia identification.

Dianguo Xu (M'97–SM'12–F'17) received the B.S. degree in control engineering from Harbin Engineering University, Harbin, China, in 1982, and the M.S. and Ph.D. degrees in electrical engineering from the Harbin Institute of Technology (HIT), Harbin, in 1984 and 1989, respectively.

In 1984, he was appointed as an Assistant Professor with the Department of Electrical Engineering, HIT, where he has been a Professor since 1994. From 2000 to 2010, he was the Dean of the School of Electrical Engineering and Automation, HIT. He is currently the Vice President of the HIT. His research interests include renewable energy generation, power quality mitigation, sensorless motor drives, and high-performance servo systems.

Dr. Xu is an Associate Editor for the IEEE TRANSACTIONS ON INDUSTRIAL ELECTRONICS.

Frede Blaabjerg (S'86–M'88–SM'97–F'03) received the Ph.D. degree in electrical engineering from Aalborg University, Aalborg, Denmark, in 1992.

He was with ABB-Scandia, Randers, Denmark, from 1987 to 1988. He was appointed an Assistant Professor in 1992, an Associate Professor in 1996, and a Full Professor of Power Electronics and Drives in 1998 with Aalborg University. His current research interests include wind turbines, photovoltaic systems, reliability, harmonics, and adjustable speed drives.

Dr. Blaabjerg was a recipient of 15 IEEE Prize Paper Awards, the IEEE PELS Distinguished Service Award in 2009, the IEEE William E. Newell Power Electronics Award 2014, and the Villum Kann Rasmussen Research Award 2014. From 2006 to 2012, he was an Editor-in-Chief for the IEEE TRANSACTIONS ON POWER ELECTRONICS. He has been a Distinguished Lecturer for the IEEE Power Electronics Society from 2005 to 2007 and for the IEEE Industry Applications Society from 2010 to 2011. He was nominated in 2014 by Thomson Reuters to be among the most 250 cited researchers in engineering in the world.